Energy Equip. Sys./ Vol. 11/No. 3/September 2023/ 305-319

ENERGY EQUIPSYS

Energy Equipment and Systems
http://energyequipsys.ut.ac.ir
www.energyequipsys.com

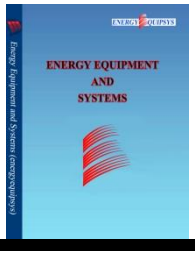

The importance of tip speed ratio on noise Pollution of H-Darrieus wind turbines

Authors

Alireza Bozorgi[a*]
Mohamad Javad Zarei[a,b]

[a]Department of Mechanical Engineering, Arak University of Technology, Arak, Iran

[b]Department of Mechanical Engineering, University of Tehran, Tehran, Iran

Article history:
Received : 8 August 2023
Accepted : 28 August 2023

ABSTRACT

Noise pollution is a significant challenge in developing the use of wind turbines, especially in residential areas. H-Darrieus turbine is a wind turbine widely used in residential areas, usually exposed to variable wind speeds, and works in a wide range of tip speed ratios. In this article, the importance of tip speed ratio on the output power and noise pollution of an H-Darrieus turbine is numerically investigated using the SST-kω model (for flow simulation at tip speed ratios of 2.04 to 3.3) and the Ffowcs Williams-Hawkings equations (for noise calculation in far-field). The directivity results show that the angle position of maximum noise differs for different tip speed ratios. Therefore, noise calculation only at the angle position of 0°, widely used for wind turbines, is insufficient. The results show that in terms of noise pollution, tip speed ratios of 2.04 and 3.3 have the best and worst performances, with maximum noises of 67.91 dB and 71.85 dB, respectively. On the other hand, the tip speed ratio of 2.64 has the highest power (2.92 times the power of 2.04) with a maximum noise of 68.26 dB, which is negligibly higher than that for the tip speed ratio of 2.04. Overall, it is concluded that in terms of compromise between noise pollution and power generation, the tip speed ratio of 2.64 is the best point for this turbine.

Keywords: Aerodynamics, CFD, Darrieus Turbine, Noise Pollution, Vertical-Axis Wind Turbine.

1. Introduction

Global wind energy capacity is predicted to exceed 1 TW by the end of 2023 and 2 TW by the end of 2030 [1]. It means the use of wind turbines will significantly increase in the future. Based on axis position, these turbines are divided into Horizontal-Axis Wind Turbines (HAWTs) and Vertical-Axis Wind Turbines (VAWTs). VAWTs, as a renewable energy source, are becoming increasingly popular. They are an attractive option for urban areas [2], having a proper price and a high suitability for complex wind conditions [3-5]. However, there are significant concerns about the noise pollution of VAWTs, especially when installed near residential areas [6]. Several researchers [7-15] investigated the effect of the noise on human health. For example, a review study carried out by Frieberg et al. [15] about the effects of wind turbines on human health concluded that exposure to the noise of wind turbines could cause annoyance, sleep disorders, mental health problems, headaches/migraines, tinnitus, dizziness/balance problems, excessive tiredness/fatigue, cardiovascular disorders, Concentration deficits, etc. Noise pollution of

* Corresponding author: Alireza Bozorgi
Department of Mechanical Engineering, Arak University of Technology, Arak, Iran
Email: bozorgi@arakut.ac.ir

VAWTs is regarded as more critical than HAWTs since VAWTs are used in residential areas. It is predicted that with increasing the use of VAWTs, their noise will constitute a significant component of urban noise [16]. VAWTs generate humming, swooshing, and whistling sounds [17-19].

National standards about the noise control of wind turbines in residential areas define different limits for noise pollution [2]. For example, in the UK, the A-weighted Sound Pressure Level (SPL) must be lower than 40 dBA for nights and lower than 50 dBA for days, while in Denmark, these limits are 50 dBA for days and 45 dBA for nights. Iran's national noise control standard defines a limit of 55 dBA for days and 45 dBA for nights in residential areas. In addition to defining the limits, effective punishment must be considered for preventing lawbreakers.

H-Darrieus Wind Turbine (HDWT) is a low-price VAWT widely used in residential areas. HDWTs have lower efficiency than HAWTs, which means they produce less energy. However, they have several advantages that make them suitable for urban areas, especially since they can capture wind from any direction. H-Darrieus turbines are also compact and have a smaller footprint than HAWTs, making them suitable for installation in areas with limited space.

Blade geometry, Tip Speed Ratio (TSR), and solidity considerably affect the aerodynamic performance of VAWTs [20-26]. For example, Mohamed et al. [20] studied the effect of blade geometry on the output power of a three-bladed HDWT using Computational Fluid Dynamics (CFD). The results exhibited that the maximum output power is for L(S)-0413 airfoil. Parakkal et al. [22] also simulated the aerodynamic performance of a three-bladed HDWT using Joukowski, NACA 0012, and NACA 4312 airfoils. They showed that the Joukowski airfoil has higher output power but a lower self-starting capability. Improving self-starting capability is essential for developing the use of HDWTs in urban environments having variable wind conditions. A numerical study by Celik et al. [24] showed that increasing the blade number improves the self-starting capability but may reduce the output power. Huang et al. [27] showed that radius reduction for part of blades improves the self-starting capability by increasing the output power in low TSRs. Studies by Abid et al. [28] and Nemati [29] exhibited that the combination of Savonius-Darrieus turbines improves self-starting capability.

Mohamed [30] investigated the effect of blade geometry on the noise of a three-bladed HDWT using S1046, FXLV152, NACA 0018, and NACA 63418 airfoils. All simulations have been performed in two dimensions using Unsteady Reynolds Averaged Navier-Stokes (URANS) and Ffowcs Williams-Hawkings (FW-H) equations [31]. The results showed that the lowest noise belongs to S1046 airfoil. Karimian et al. [32] studied the effect of pitch angle on the output power and noise of an HDWT and showed that a change in pitch angle may oppositely affect output power and noise pollution.

Ghasemian et al. [33] simulated the noise pollution of an HDWT in three dimensions. They concluded that the noise reduces with a logarithmic trend when observer distance increases.

In this article, the effect of TSR on the noise pollution of an HDWT is studied to find a compromise between output power and noise pollution. For this purpose, the flow is first simulated in two dimensions using the URANS equations and the SST-kω model. Then the noise received by observers is calculated using the FW-H equations. In most past studies, observers have been defined in only one angle position (in wind direction and downstream of turbines) [30, 32-33]. However, maximum noise may be in another angle position, and a directivity pattern must be investigated to find it. In the present work, a directivity pattern is obtained, using several observers on a full circle, to find the angle position and SPL of maximum noise.

Nomenclature

C_p	Pressure coefficient
c_0	Speed of sound (m/s)
L_i	Dipole sources
P	Output power (W)
P_{ij}	Compressive stress tensor (Pa)
Q	Monopole sources
R	Rotor radius (m)
T	Time period (s)

T_{ij} Quadrupole sources
u Flow velocity (m/s)
U Wind speed (m/s)
V_n Normal component of data surface velocity (m/s)

Greek Symbols
ρ Density (kg/m^3)
σ_{ij} Viscous stress tensor (Pa)
ω Rotational speed (rad/s)

2. Aerodynamic Simulation

Aerodynamic simulation was performed to calculate the power coefficient C_p at TSRs of 2.04 to 3.3 and also to extract noise sources. C_p and TSR are given by

$$C_p = \frac{P}{\left(\frac{1}{2}\rho U^3 A\right)}; A = 2RL \tag{1}$$

$$TSR = \frac{R\omega}{U} \tag{2}$$

In Eqs. (1) and (2), P is output power, ρ air density, U wind speed, R rotor radius, L rotor height, and ω rotational speed. The benchmark HDWT is a three-bladed turbine whose blade profile corresponds to NACA 0021 airfoil. The geometric properties of this turbine and operational conditions have been listed in Table 1.

The numerical simulation was performed using the two-dimensional continuity and URANS equations for incompressible flow, given by

$$\frac{\partial \overline{u_i}}{\partial x_i} = 0 \tag{3}$$

$$\rho\left(\frac{\partial \overline{u_i}}{\partial t} + \frac{\partial \overline{u_i u_j}}{\partial x_j}\right) = -\frac{\partial \overline{p}}{\partial x_i} + \frac{\partial}{\partial x_i}\left(\mu\left(\frac{\partial \overline{u_i}}{\partial x_j} + \frac{\partial \overline{u_j}}{\partial x_i}\right)\right) - \rho\overline{u_i' u_j'} \tag{4}$$

In Eqs. (3) and (4), $\overline{u_i}$ and $\overline{p}$ denote mean velocity components and mean pressure, respectively. Here, the Reynolds stress term, given by $\rho\overline{u_i' u_j'}$, is solved using the SST-kω model. This turbulence model was developed by Menter [34] to blend the robustness of the k-ω model in near-wall region with the free-stream independence of the k-ε model in far-field.

Table 1. Geometric properties and operating conditions

Parameter	value
Rotor diameter	1.03 m
Number of blades	3
Blade chord	85.8 mm
Wind speed	9 m/s
TSR	2.04 to 3.3

Flow domain and boundary conditions are shown in Fig. 1a. According to investigations of Mohamed et al. [35], the domain must spread more than ten times the rotor diameter in all directions. This condition has been met in the current simulation. The domain was divided into rotary and stationary subdomains connected to each other with an interface boundary condition. Boundary layer mesh was applied on blade walls (Fig. 1b) such that the mean of Y+ on the wall of the blades was 1.7, an agreeable value for the SST-kω model. In Fig. 2, Y+ on the walls has been shown. Velocity inlet and pressure outlet boundary conditions were used for the upstream and the downstream, respectively. Mesh independency was checked using grid sizes from 50.928 to 392.158 cells. The study revealed that the relative deviation of C_p calculation was less than 1% (Fig. 3). Here, the grid size of 177,541 cells was selected for all simulations to reduce computational cost. In this grid, the average orthogonal quality on the stationary and rotating zones was 0.980 and 0.942, respectively, and the equivolume skewness on the stationary and rotating zones was 0.024 and 0.086, respectively.

The SIMPLE algorithm was applied for pressure-velocity coupling and the Green-Gauss cell-based method for gradient calculation. The second-order upwind method was used to discretize convection terms and turbulence equations, the second-order method for pressure terms, and the second-order implicit method for transient terms.

Each time period was divided into 128 time-steps with 20 internal iterations per one time-step. Therefore, a full rotation of the turbine has been divided into 384 time-steps. It means the turbine rotated less than one degree in each time-step. The simulations were performed for at least ten revolutions, although the results converged after five revolutions.

The Cp-TSR curve of the current work and

other numerical simulations [20-21, 36-38] has been compared with experiment [36] in Fig. 4. It is observed that the curve of the current work is the nearest to the experiment. This comparison confirms that the current numerical simulation is agreeable for predicting the aerodynamic performance of this turbine.

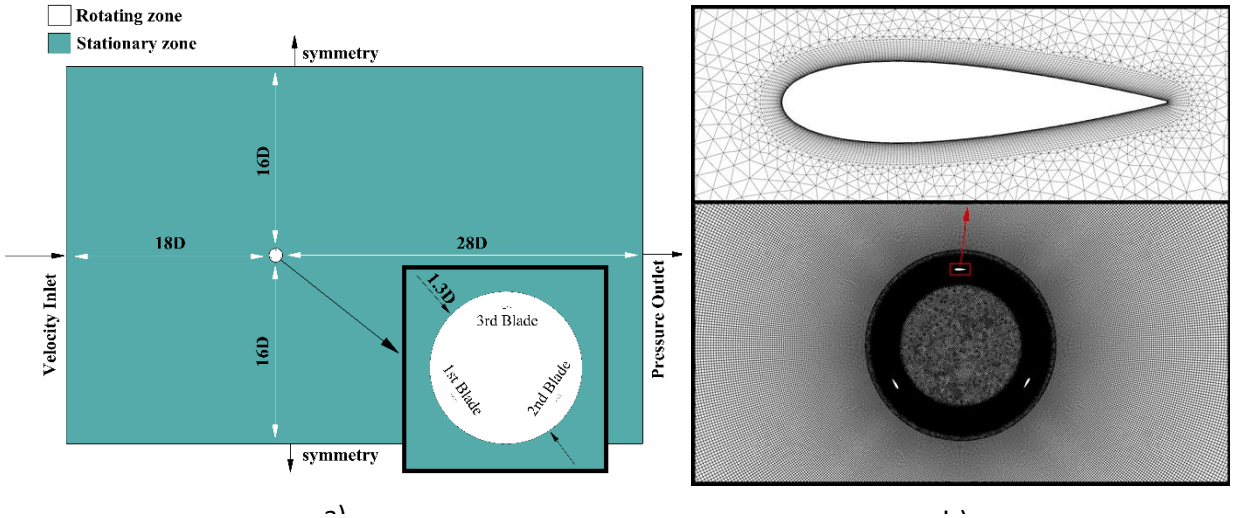

Fig. 1. a) Flow domain b) mesh

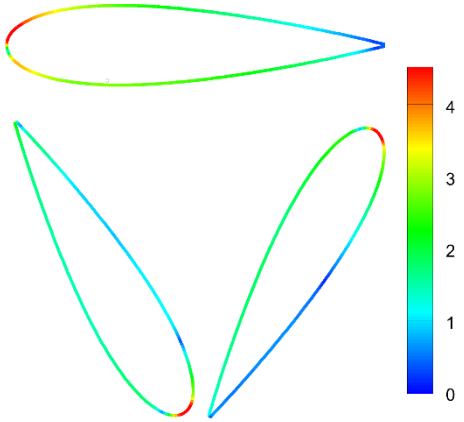

Fig. 2. Y+ on Blades for TSR = 2.64

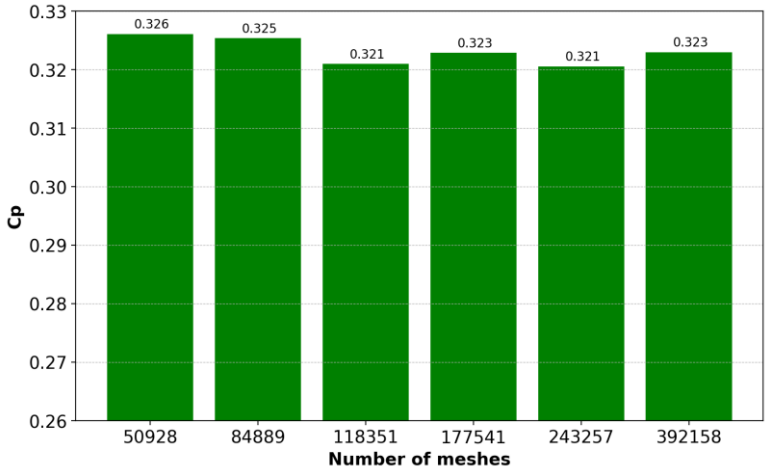

Fig. 3. Mesh independence study at TSR = 2.64

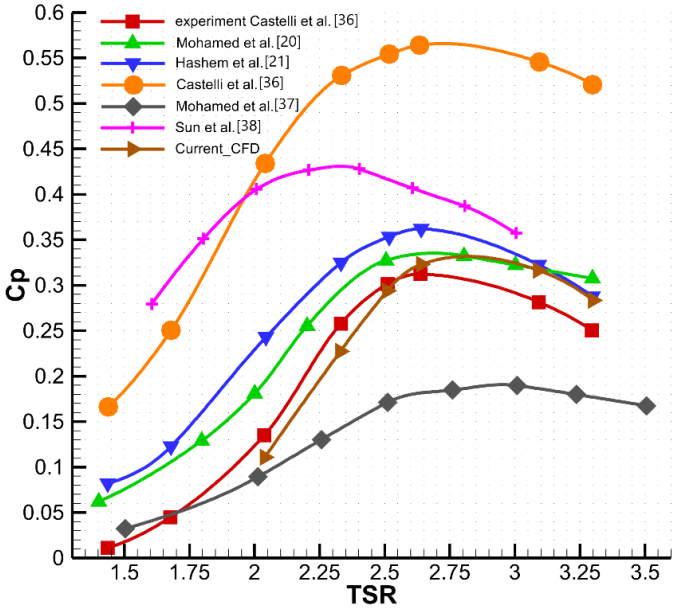

Fig. 4. Comparison of aerodynamic results

According to Betz's law, the upper limit of C_p in wind turbines is 0.593. An experimental and numerical study by Ranjbar et al. [39] showed that it is possible to reach this limit, but practically the C_p is still less than this value, especially in VAWTs. For example, Fadil et al. [40] compared a VAWT and a HAWT having an identical swept area of 3.14 m^2 and three blades with NACA 4412 profile. They showed that there is a considerable difference between the C_p of the VAWT and the HAWT. The maximum C_p for the VAWT was 0.34, while for the HAWT, it was 0.54.

3. Noise Calculation

The noise propagated from the blades of the HDWT was calculated using the FW-H equations [31], widely used for calculating the noise of moving bodies. The equation for solid walls as data surface (where f = 0) is given by

$$\left\{\frac{1}{c_0^2}\frac{\partial^2}{\partial t^2}-\frac{\partial^2}{\partial x_i^2}\right\}\left[p'(\mathbf{x},t)H(f)\right]= \frac{\partial}{\partial t}\left[Q\delta(f)\right]-\frac{\partial}{\partial x_i}\left[L_i\delta(f)\right]+\frac{\partial^2}{\partial x_i\partial x_j}\left[T_{ij}H(f)\right] \quad (5)$$

$$Q=\rho_0 v_n \qquad L_i=P_{ij}n_j \qquad T_{ij}=\rho u_i u_j+\left(p-p_0-c_0^2(\rho-\rho_0)\right)\delta_{ij}-\sigma_{ij} \quad (6)$$

In Eqs. (5) and (6), p' is pressure fluctuations, H(f) the step function, δ(f) the Dirac delta function, and c_0 the speed of sound. Q, L_i and T_{ij} represent monopole, dipole and quadrupole sources, respectively. v_n denotes the normal component of data surface velocity. P_{ij} is the compressive stress tensor, σ_{ij} the viscous stress tensor, and n_j the j-th component of normal unit vector at the data surface. A "0" subscript denotes mean quantities.

Ansys Fluent uses formulation 1A of Farassat [41], an integral FW-H equation solution, for noise calculation. In the setting box, the far-field density was defined as equal to 1.225 kg/m3, the speed of sound 340 m/s, and the reference pressure 2e-5 Pa. Moreover, the convective effect option was activated, which corrects the value of c_0 affected by wind speed (mean flow). Finally, 12 observers were defined on a full circle with a 10 m radius (Fig. 5).

4. Results and Discussion

The directivity pattern of the rotor (interaction of all blades) is shown in Fig. 6. The SPL was calculated by

$$SPL=20\frac{P_{rms}}{P_{ref}} \quad (7)$$

where P_{rms} is the root mean square of pressure fluctuations in a full turbine rotation, and P_{ref} is equal to 2e-5 Pa. All observers were located at R = 10 m with a 30° difference in angle position.

It is observed that the directivity profile and also the angle position of maximum noise (the most critical point) depend on TSR. The maximum and minimum noise of the rotor has been listed in Table 2 to determine the range of SPL on the circle with R = 10 m. The highest difference is for the TSR of 2.04, equal to 6.43 dB, while the lowest is for the TSR of 2.51, equal to 4.51 dB.

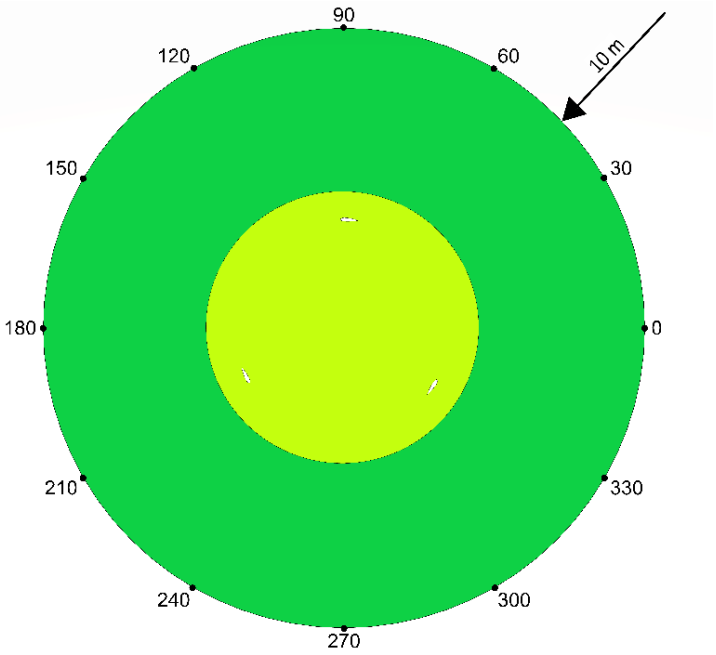

Fig. 5. The position of observers

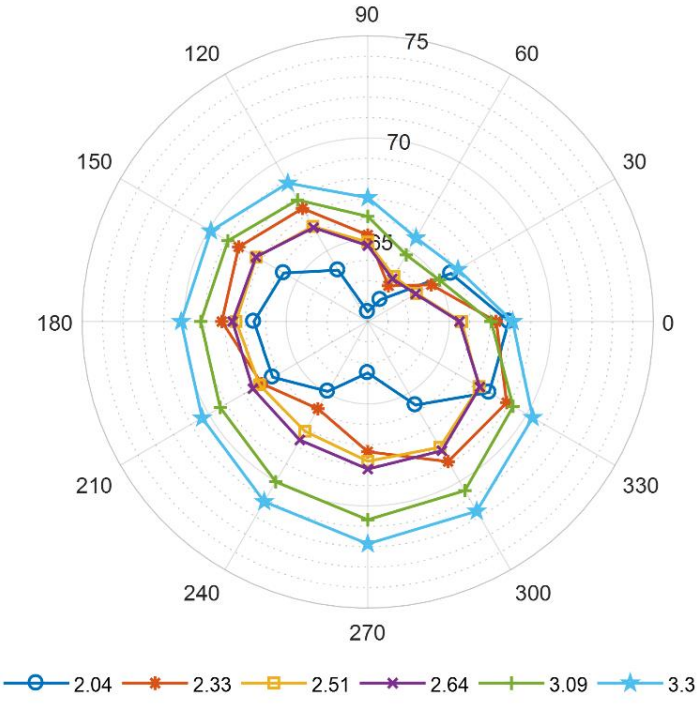

Fig. 6. Directivity pattern for the rotor in different TSRs

Table 2. Performance of the HDWT

TSR	Cp	Max. noise		Min. noise	
		SPL (dB)	θ	SPL (dB)	θ
2.04	0.1107	67.91	0°	61.48	90°
2.33	0.2274	68.88	300°	63.02	60°
2.51	0.2940	68.07	300°	63.56	60°
2.64	0.3229	68.26	300°	63.42	60°
3.09	0.3164	70.67	270°	64.77	60°
3.30	0.2833	71.85	270°	65.73	60°

According to the IEC 61400-11 standard [42], only a necessary point is defined for noise measurement having $\theta = 0^{\circ}$. In most research works, the noise has also been calculated at only $\theta = 0^{\circ}$ as a routine angle position. However, the results in Table 2 show that the angle only for TSR=2.04 is at $\theta = 0^{\circ}$, but for TSR = 2.33, 2.51, 2.64 is at $\theta = 270^{\circ}$, and for TSR = 3.09, 3.33 is at $\theta = 330^{\circ}$. Therefore, the angle position of maximum noise is not identical in all TSRs. It is concluded that noise calculation at only one angle position cannot be reliable for finding the maximum noise of HDWTs, and for this purpose, directivity must be determined. HDWTs are appropriate for use in areas with variable wind direction. Therefore, the directivity profile rotates if wind direction changes, which means the maximum noise can be located at any angle position.

The results in Table 2 show that the least noise pollution is for TSR = 2.04 with a maximum noise of 67.91 dB and the most for TSR = 3.3 with a maximum noise of 71.85 dB. However, the maximum C_p is for TSR = 2.64, about three times that for TSR = 2.04 (2.92 times), while the maximum noise increases less than 0.5 dB. In terms of compromise between noise pollution and power generation, the TSR of 2.64 is the best point for this turbine.

If the noise sources of all three blades coincide in place and time, the rotor noise is three times blade noise, equaling to a 9.54 dB increase in the rotor noise (according to Eq. (7)). The directivity of the rotor and of one of the blades is compared to each other in Fig. 7. The results show that the noise of the rotor is higher than that of the blade, which means the interaction of the blades amplifies the noise pollution. However, the increase is less than 9.54 dB in all observer positions since there is a phase difference between the noise of the blades. The phase difference between the noise of the blades is equal to $2\pi/3$ rad. The time history of the noise for the rotor and one of the blades in a full rotation is shown in Fig. 8. It is observed that the waveform of the blade noise changes when the observer position changes. Subsequently, the waveform of the rotor noise, which is the sum of the noise of the blades, depends on the observer position. Moreover, as shown in Fig. 8, the rotor noise is not a sinusoidal function, which means the noise is not tonal. The investigation of frequency distribution can determine significant frequencies of the noise received by the observers. For this purpose, a Fast Fourier Transform (FFT) was carried out on the noise. Figure 9 displays the frequency distribution based on rotor frequency ($f_{rotor} = \omega/2\pi$) for some observer positions. It is observed that the first peak is located at three times the rotor frequency, which is as equal to Blade Passing Frequency (BPF)

$$\text{BPF} = \text{blade numbers} \times \frac{\omega(\text{rad/s})}{2\pi} \tag{8}$$

Other peaks are in the next BPFs but have a lower SPL. The results show that the frequency distribution differs for different observers and TSRs. It can change the type of sound heard by observers, such as humming, swooshing, whistling, etc. Therefore, in addition to directivity, frequency distribution must be checked to have a comprehensive study on the noise behavior of this turbine.

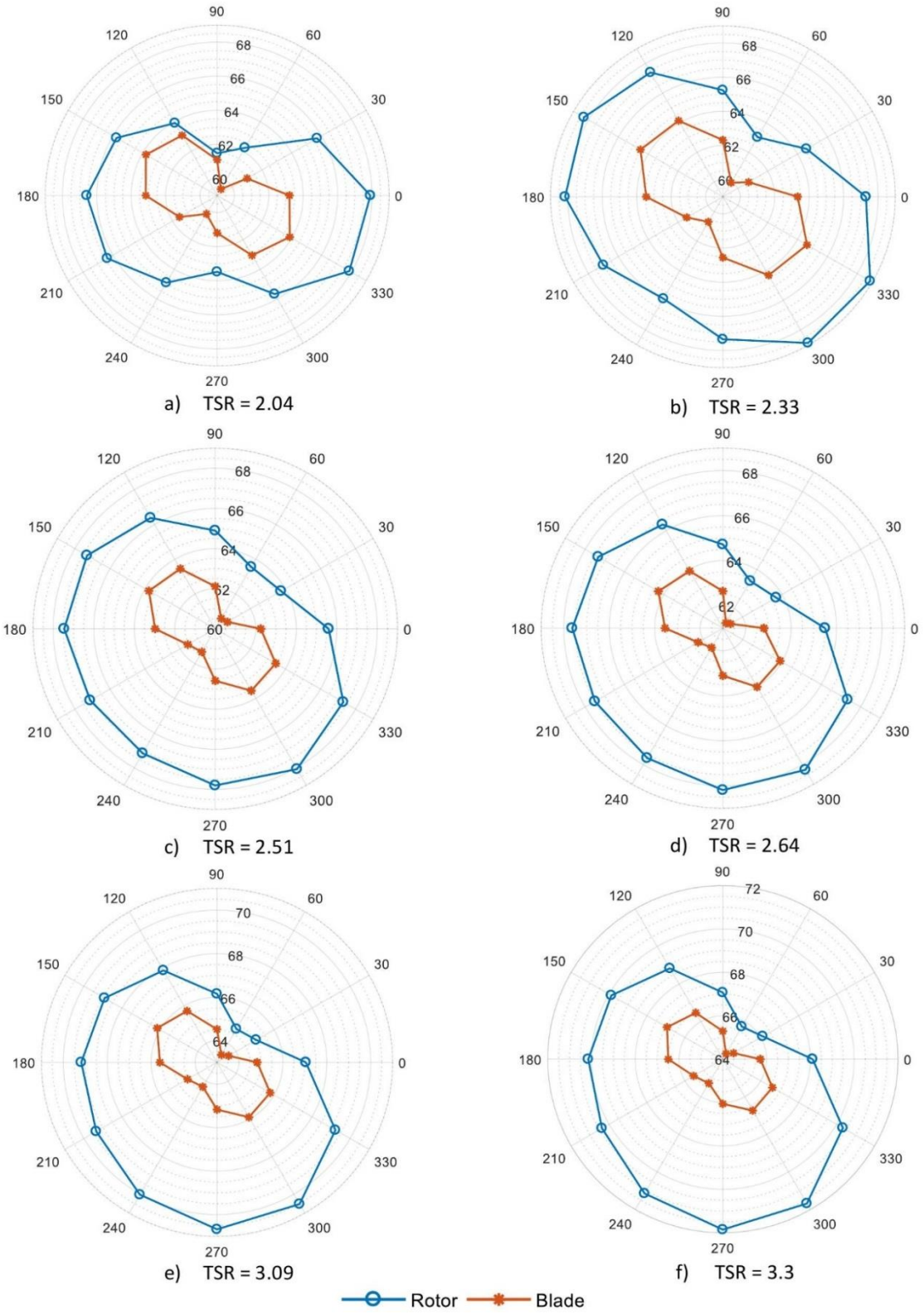

Fig. 7. Comparing the directivity of the rotor and one of the blades

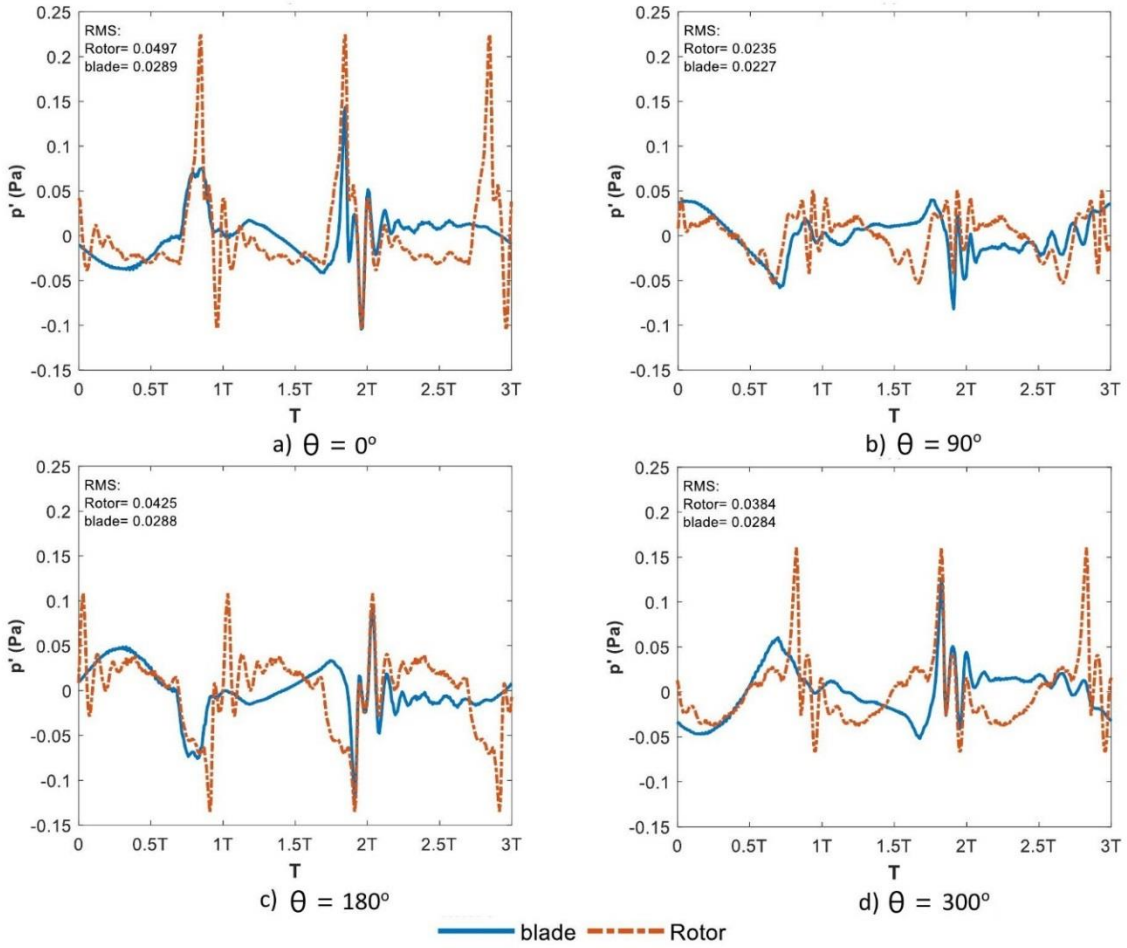

Fig. 8. Time history of the noise for TSR = 2.04 in different observer positions

As shown in Eq. (6), monopole noise source depends only on blade wall and is independent of flow, but dipole and quadrupole noise sources depend on flow. Dipole noise source depends on pressure distribution around blade wall. Figure 10 displays the pressure contour for all TSRs at t = 0.680943 s. The results show that the pressure distribution in the flow domain significantly changes with the TSR. Moreover, it is observed that at each specified TSR, pressure distribution around the blades is different from each other. Therefore, dipole noise sources on the blades are different from each other at identical times; unlike HAWTs, the flow is symmetrical and dipole noise sources on blades are identical.

Quadrupole noise sources represent the effect of vortices and wake on noise generation [43-44]. Overall, it is expected that the quadruple sources intensify noise pollution. Figure 11 shows vorticity contours for all TSRs. A qualitative comparison shows that vortex shedding at the TSR of 2.04 is stronger than it at 2.64. It means quadrupole sources can further intensify the noise pollution in the TSR of 2.04, that it reduces or even can destroy the slight advantage of less noise pollution (less than 0.5 dB (Table 2)) for this TSR in comparison with the TSR of 2.64. In order to capture vortices with proper accuracy, the flow must be three-dimensionally simulated with a high mesh resolution that multiplies the computational cost.

It is observed that the vortex shedding from the 1st blade affects the 3rd blade (blade numbering is according to Fig. 1), which can significantly affect the aerodynamic performance of this blade. It is one of the reasons that the C_p of VAWTs is lower than the C_p of HAWTs.

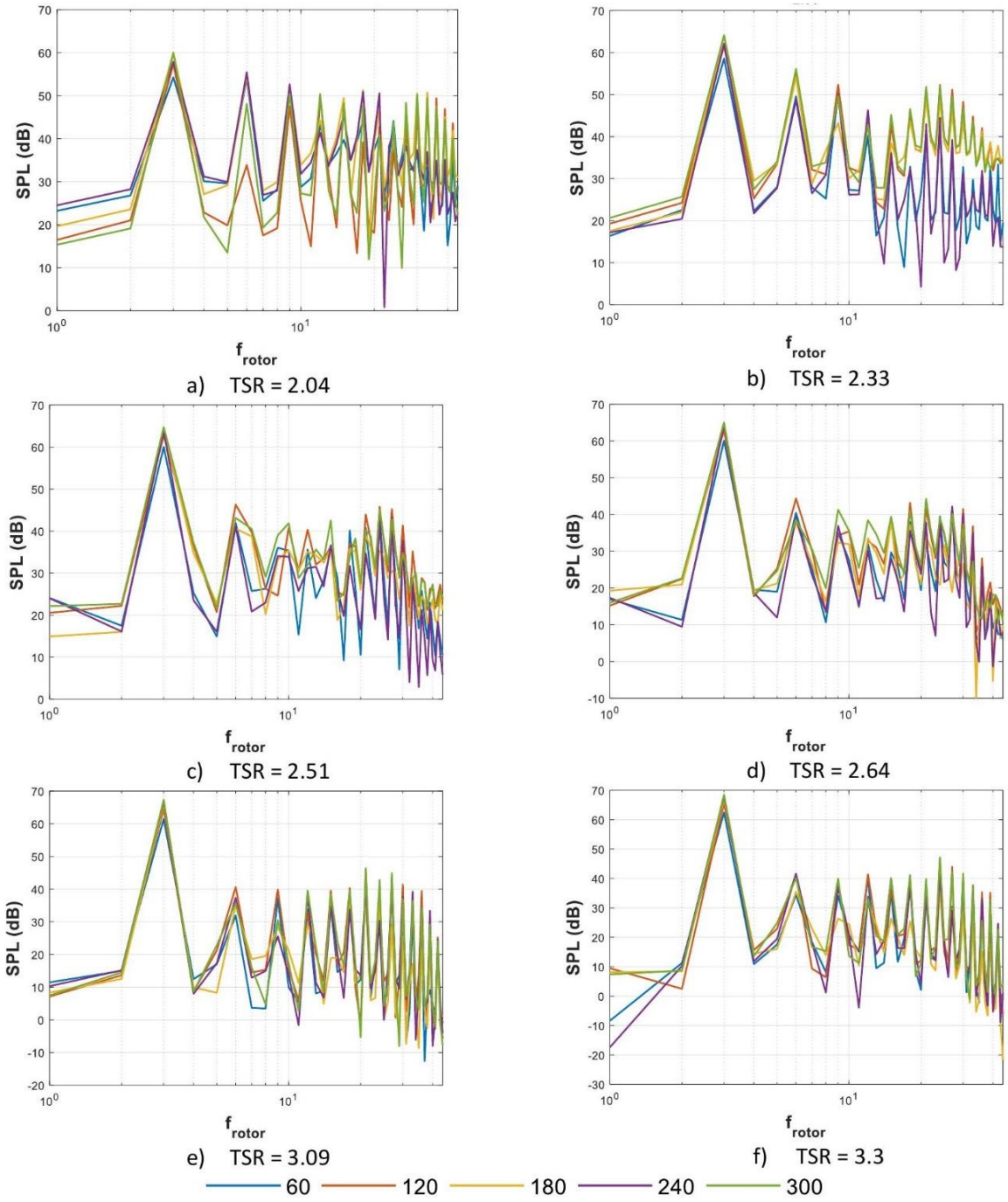

Fig. 9. Frequency distribution for different observer positions

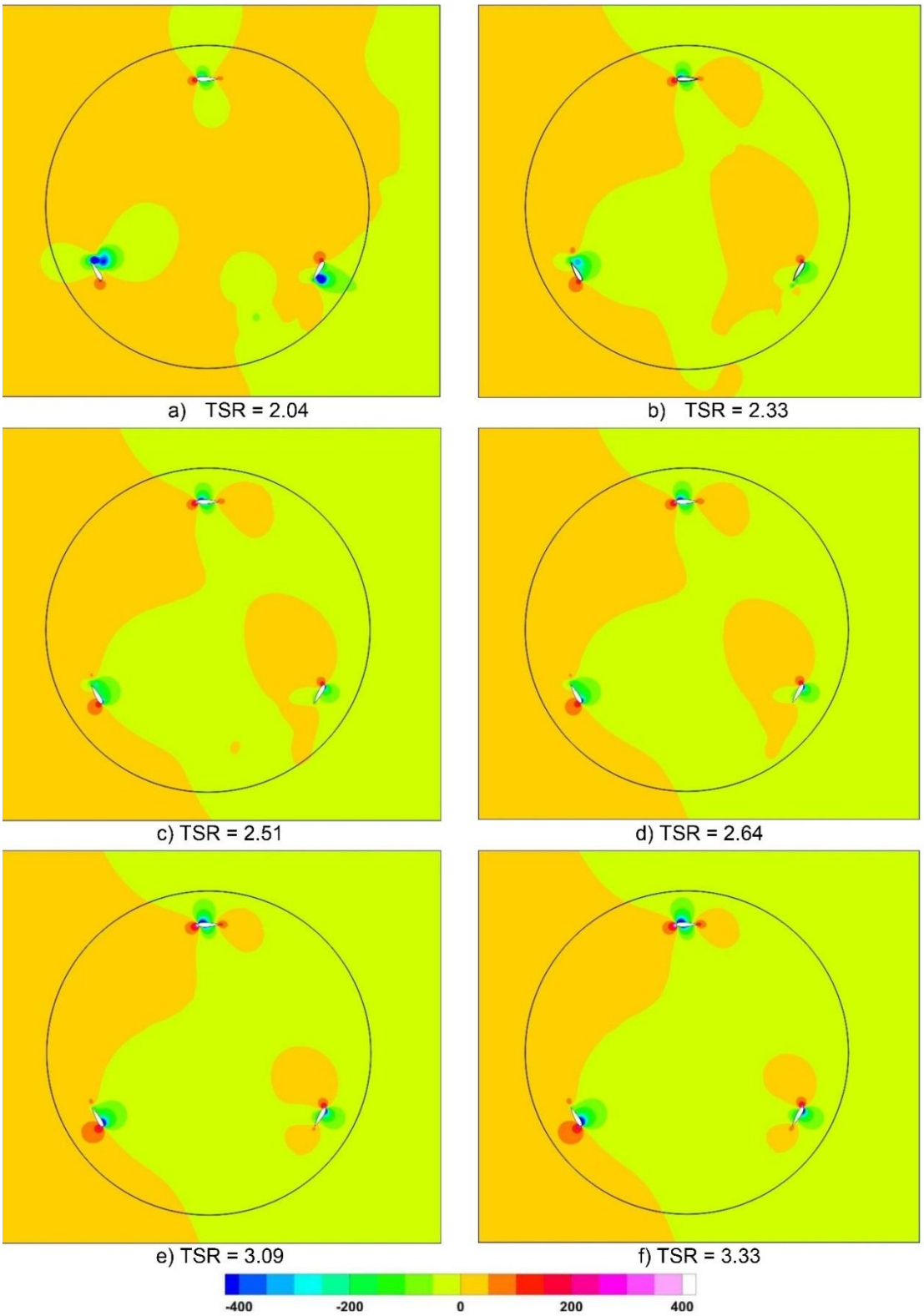

Fig. 10. Pressure contour for different TSRs

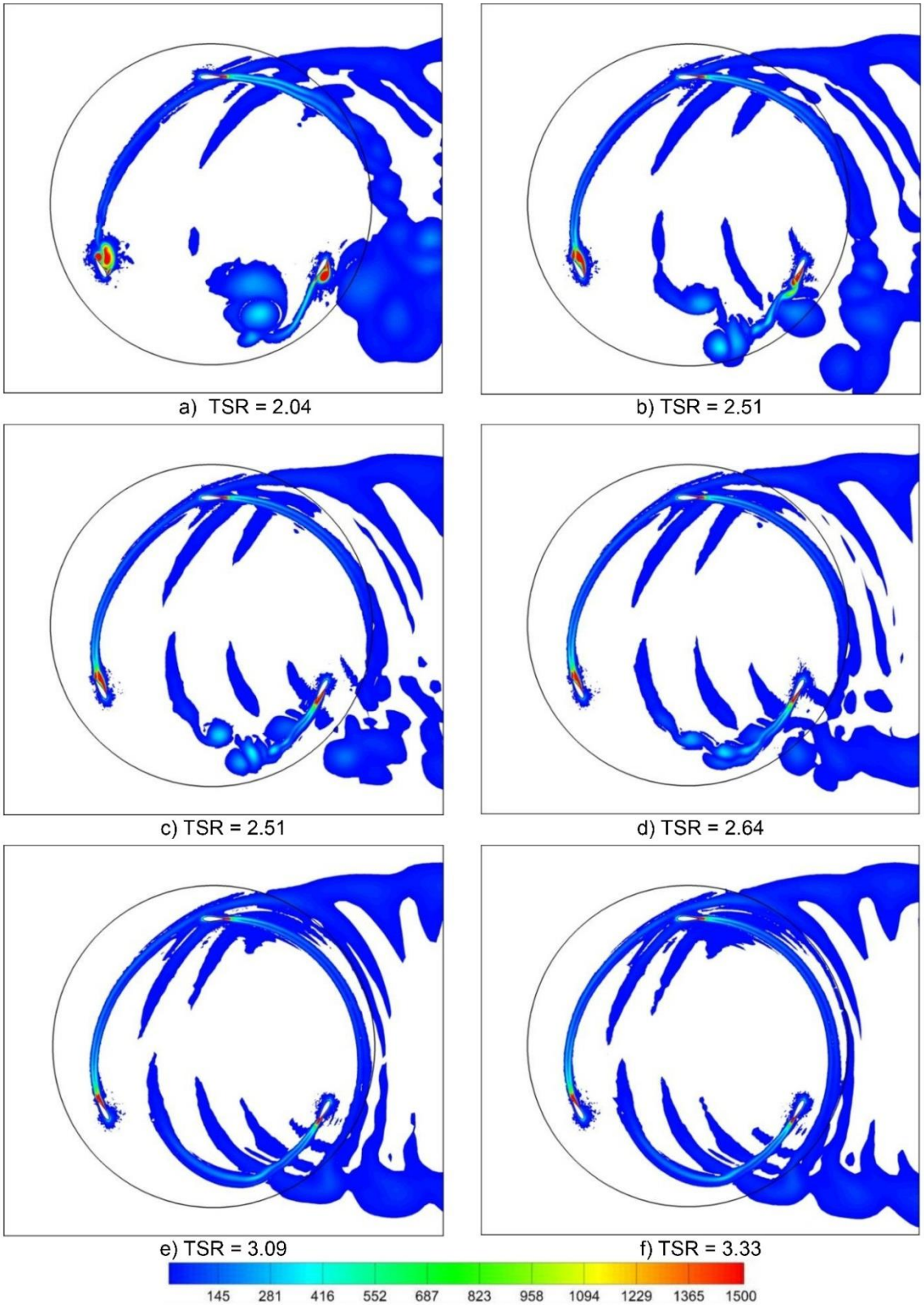

Fig. 11. Vorticity contour for different TSRs

5. Conclusion

In this article, the importance of TSR on the output power and noise pollution of HDWTs was investigated using CFD. For this purpose, flow around a benchmark HDWT was first simulated using the SST-kω turbulence model. It was observed that the numerical results of the present work are in very good agreement with the experiment compared to other numerical works. In the next, the FW-H equations were applied to calculate SPL in 12 observer points located on a circle with a 10 m radius .

The results showed that TSR significantly affects noise pollution. The most noise pollution was for the TSR of 3.3, with a maximum noise of 71.85 dB, and the least was for the TSR of 2.04, with a maximum noise of 67.91 dB, while the maximum C_p was for the TSR of 2.64. A change in the TSR from 2.04 to 2.64 increased the C_p 2.92 times, while it led to less than 0.5 dB increase in the maximum noise that is negligible. Overall, regarding the compromise between noise pollution and power generation, the TSR of 2.64 was introduced as the best point for this turbine .

Moreover, it was observed that the angle position of maximum noise is not identical in all TSRs. The angle position for the TSR of 2.04 was at $\theta = 0^{o}$, for TSRs of 2.33, 2.51 and 2.64 was at $\theta = 270^{o}$, and for TSRs of 3.09 and 3.3 was at $\theta = 330^{o}$. The results showed that noise calculation only at $\theta = 0^{o,}$ which is routine in the noise calculation of wind turbines, is insufficient for finding the maximum noise.

The results showed that the rotor noise received by the observers is not a sinusoidal function, which means the noise is not tonal. The investigation of frequency distribution exhibited that the highest peak is at the first BPF for all cases, but the frequency distribution differs when the observer position or TSR changes. It means the type of sound heard by observers, such as humming, swooshing, whistling, etc., depends on the angle position. Therefore, in addition to directivity, frequency distribution must be checked to have a comprehensive study on the noise behavior of this turbine.

Finally, the investigation of vorticity contours showed that the vortex shedding of each blade affects other blades. It can be one of the reasons that VAWTs have lower Cp in comparison with HAWTs.

References

[1] Council–GWEC, Global wind report 2023, (2023), Global Wind Energy Council.

[2] Li S., Chen Q., Li Y., Pröbsting S., Yang C., Zheng X., Yang Y., Zhu W., Shen W., Wu F., Li D., Experimental investigation on noise characteristics of small scale vertical axis wind turbines in urban environments, Renewable Energy (2022) 200: pp. 970-982.

[3] Barnes A., Hughes B., Determining the impact of VAWT farm configurations on power output, Renewable energy (2019) 143: pp. 1111-1120.

[4] Rezaeiha A., Montazeri H., Blocken B., A framework for preliminary large-scale urban wind energy potential assessment: Roof-mounted wind turbines, Energy Conversion and Management (2020) 214: p. 112770.

[5] Xu W., Li Y., Li G., Li S., Zhang C., Wang F., High-resolution numerical simulation of the performance of vertical axis wind turbines in urban area: Part II, array of vertical axis wind turbines between buildings, Renewable Energy (2021)176: pp. 25-39.

[6] Pedersen E., Persson Waye K., Perception and annoyance due to wind turbine noise—a dose–response relationship, The Journal of the Acoustical Society of America (2004) 116: pp. 3460-3470.

[7] Arra I., Lynn H., Barker K., Ogbuneke C., Regalado S., Systematic Review 2013: Association between wind turbines and human distress, Cureus (2014) 6.

[8] Colby D., Dobie R., Leventhall G., Lipscomb D.M., McCunney R.J., Seilo M.T., Sondergaard B., Wind turbine sound and health effects: An expert panel review, (2009), American Wind Energy Association and Canadian Wind Energy Association.

[9] Farboud A., Crunkhorn R., Trinidade A., 'Wind turbine syndrome': fact or fiction?, The Journal of Laryngology & Otology(2013) 127: pp. 222-226.

[10] Jeffery R.D., Krogh C.M.E., Industrial wind turbines and adverse health effects, Canadian journal of rural medicine, (2014) 19: pp. 21-26.
[11] Knopper L.D., Ollson C.A., Health effects and wind turbines: A review of the literature, Environmental health (2011) 10: pp. 1-10.
[12] Kurpas D., Mroczek B., Karakiewicz B., Kassolik K., Andrzejewski W., Health impact of wind farms, Annals of Agricultural and Environmental Medicine (2013) 20.
[13] Onakpoya I.J., O'Sullivan J., Thompson M.J., Heneghan C.J., The effect of wind turbine noise on sleep and quality of life: A systematic review and meta-analysis of observational studies, Environment international (2015) 82: pp. 1-9.
[14] McCunney R.J., Mundt K.A., Colby W.D., Dobie R., Kaliski K., Blais M., Wind turbines and health: A critical review of the scientific literature, Journal of occupational and environmental medicine (2015) 57: pp. 133-135.
[15] Freiberg, A., Schefter C., Girbig M., Murta V.C., Seidler A., Health Effects of Wind Turbines on Humans in Residential Settings: Results of a Scoping Review, Environmental research (2019) 169: pp. 446-463.
[16] Tsai D.Y., Hsu H.Y., Chen G.E., Ting C.C., Developing the Full-Field Wind Generator Integrated with the Vertical Twin Rotors, International Journal of Electrical Power & Energy Systems (2018) 103: pp. 395-403.
[17] Möllerström E., Larsson S., Ottermo F., Hylander J., Bååth L., Noise propagation from a vertical axis wind turbine, In inter. noise 2014, 43rd International Congress on Noise Control Engineering (2014) Nov. 16-19, 43: pp.
[18] Taylor J., Eastwick C., Lawrence C., Wilson R., Noise levels and noise perception from small and micro wind turbines, Renewable Energy (2013) 55: pp. 120-127.
[19] Waye K.P., Öhrström E., Psycho-acoustic characters of relevance for annoyance of wind turbine noise, Journal of sound and vibration (2002) 250: pp. 65-73.
[20] Mohamed M., Dessoky A., Alqurashi F., Blade Shape Effect on the Behavior of the H-Rotor Darrieus Wind Turbine: Performance Investigation and Force Analysis, Energy (2019) 179: pp. 1217-1234.
[21] Hashem I., Mohamed M., Aerodynamic Performance Enhancements of H-Rotor Darrieus Wind Turbine, Energy (2018) 142: pp. 531-545.
[22] Parakkal J.U., EI. Kadi K., El-Sinawi A., Elagroudy S., Janajreh I., Numerical Analysis of VAWT Wind Turbines: Joukowski Vs Classical NACA Rotor's Blades, Energy Procedia (2019) 158: pp. 1194-1201.
[23] Singh M., Biswas A., Misra R., Investigation of Self-Starting and High Rotor Solidity on the Performance of a Three S1210 Blade H-Type Darrieus Rotor, Renewable energy (2015) 76: pp. 381-387.
[24] Celik Y., Ma L., Ingham D., Pourkashanian M., Aerodynamic Investigation of the Start-up Process of H-Type Vertical Axis Wind Turbines Using CFD, Journal of Wind Engineering and Industrial Aerodynamics (2020) 204: p. 104252.
[25] Tong G., Li Y., Tagawa K. Feng F., Effects of Blade Airfoil Chord Length and Rotor Diameter on Aerodynamic Performance of Straight-Bladed Vertical Axis Wind Turbines by Numerical Simulation, Energy (2023) 265: p. 126325.
[26] Maalouly M., Souaiby M., ElCheikh A., Issa J. Elkhoury M., Transient Analysis of H-Type Vertical Axis Wind Turbines Using CFD, Energy Reports (2022) 8: pp. 4570-4588.
[27] Huang, H., Li j., Li G., Improving the Self-Starting and Operating Characteristics of Vertical Axis Wind Turbine by Changing Center Distance in Part of Blades, Journal of Building Engineering (2023) 68: p. 105974.
[28] Abid M., S. Karimov K., A. Wajid H., Farooq F., Ahmed H., H. Khan O., Design, Development and Testing of a Combined Savonius and Darrieus Vertical Axis Wind Turbine, Iranian (Iranica) Journal of Energy & Environment (2015) 6: pp. 1-4.
[29] Nemati A., Three-Dimensional

Numerical Study of the Performance of a Small Combined Savonius-Darrieus Vertical Wind Turbine, Iranian (Iranica) Journal of Energy & Environment (2020) 11: pp. 163-169.

[30] Mohamed M., Aero-Acoustics Noise Evaluation of H-Rotor Darrieus Wind Turbines, Energy (2014) 65: pp. 596-604.

[31] Ffowcs Williams J.E., Hawkings D.L., Sound generation by turbulence and surfaces in arbitrary motion, Philosophical Transactions of the Royal Society of London. Series A, Mathematical and Physical Sciences (1969) 264: pp. 321-42.

[32] Karimian S., Rasekh S., Power and noise performance assessment of a variable pitch vertical axis Darrieus type wind turbine, Journal of the Brazilian Society of Mechanical Sciences and Engineering (2021) 43: p. 437.

[33] Ghasemian M., Nejat A., Aero-Acoustics Prediction of a Vertical Axis Wind Turbine Using Large Eddy Simulation and Acoustic Analogy, Energy (2015) 88: pp. 711-717.

[34] Menter, F.R., Review of the Shear-Stress Transport Turbulence Model Experience from an Industrial Perspective, International journal of computational fluid dynamics (2009) 23: pp. 305-316.

[35] Mohamed M.H., Janiga G., Pap E., Thévenin D., Optimal blade shape of a modified Savonius turbine using an obstacle shielding the returning blade, Energy Conversion and Management (2011) 52: pp. 236-242.

[36] Castelli M.R., Englaro A., Benini E., The Darrieus Wind Turbine: Proposal for a New Performance Prediction Model Based on CFD. Energy (2011) 36: pp. 4919-4934.

[37] Mohamed M., Ali A., Hafiz A., CFD Analysis for H-Rotor Darrieus Turbine as a Low Speed Wind Energy Converter, Engineering Science and Technology, an International Journal (2015) 18: pp. 1-13.

[38] Sun X., Wang Y., An Q., Cao Y., Wu G., Huang D., Aerodynamic performance and characteristic of vortex structures for Darrieus wind turbine. I. Numerical method and aerodynamic performance, Journal of Renewable and Sustainable Energy (2014) 6, pp. 1-12.

[39] Ranjbar M.H., Nasrazadani S.A., Zanganeh Kia H., Gharali K., Reaching the Betz limit experimentally and numerically, Energy Equipment and Systems (2019) 7: pp. 271-278.

[40] Fadil J., Ashari M., Performance comparison of vertical axis and horizontal axis wind turbines to get optimum power output. In 2017 15th international conference on quality in research (QiR): International symposium on electrical and computer engineering 2017 Jul. 24, 15 (pp. 429-433).

[41] Farassat, F., Derivation of Formulations 1 and 1A of Farassat, (2017).

[42] IEC, IEC 61400-11 Wind turbines Part 11: Acoustic noise measurement techniques, (2012) International Electrotechnical Commission.

[43] Farassat, F., Quadrupole Source in Prediction of the Noise of Rotating Blades-a New Source Description, 11th Aeroacoustics Conference (1987) Oct. 1: p. 2675.

[44] Farassat, F., Brentner K.S., The Uses and Abuses of the Acoustic Analogy in Helicopter Rotor Noise Prediction. Journal of the American Helicopter Society (1988) 33: pp. 29-36.